The interaction of water with *cis* and *trans* $\{Ru(bpy)_2(PTA)_2\}^{2+}$ (PTA = 1,3,5-triaza-7-phosphaadamantane) studied by neutron scattering and *ab initio* calculations.

Franco Scalambra,[a] Nicole Holzmann[b], Leonardo Bernasconi[c], Silvia Imberti[d], Antonio Romerosa*[a]

Abstract: The nature of the interaction of water molecules with $[Ru(bpy)_2(PTA)_2]Cl_2$ (**1Cl₂**) and *trans*-$[Ru(bpy)_2(PTA)_2]F_2$ (**2F₂**) in aqueous solution was studied using neutron scattering and electronic structure calculations. Both complexes were obtained in grams by a new synthetic procedure, and their response to UV-vis radiation was examined using calculations. The new complex **2F₂** was characterized by elemental analysis, NMR and IR spectroscopy. Complex **2F₂** was also fully characterized by single crystal X-ray diffraction. An analysis of the solvent distribution around the complexes, based on neutron diffraction data and *ab initio* calculations was used to study the solvent distribution around the two complexes, and to link the solvent environment to specific features in the optical response of their solutions.

Introduction

Ruthenium bisbipyridyl (bpy) complexes $\{Ru(bpy)_2L^1L^2\}^{x+}$ have been attracting attention for decades because of their photochemical properties, which are important for their use as photosensitizers, antitumoral prodrugs and catalysts.[1–7] The photochemistry of this family of complexes strongly depends on the ligands L^1 and L^2, which modify the electronic density distribution in the vicinity of the ruthenium centre. Interactions of the ligands with other molecules usually produce modifications in their structure and electronic distribution and therefore the coordination environment of the complex can also affect the metal and modulate the complex properties. For example, ligands containing acidic or basic groups can affect the optical properties of the complexes, leading to on-off fluorescent pH-sensitive switches,[8–12] which can be useful as sensors for the intracellular environment and as imaging tools.[13]

Recently, we synthesised the complexes *cis*-$[Ru(bpy)_2(PTA)_2]Cl_2$ (**1Cl₂**) and *trans*-$[Ru(bpy)_2(PTA)_2]OTf_2$ (**2(CF₃SO₃)₂**) (PTA = 1,3,5-triaza-7-phosphaadamantane, OTf = $CF_3SO_3^-$), whose photophysical and photochemical properties in aqueous solution have been found to depend on the pH.[14] Unfortunately, it was not possible characterise fully their luminescence properties due to their low quantum yield and short excited-state lifetime. It is known that protic solvents quench molecular luminescence through non-radiative decay promoted by hydrogen bonds and electron transfers.[15,16] Interactions usually occur at specific molecular sites and knowledge of the solvent location around the fluorophore is therefore crucial in the determination of the quenching mechanism. A deep knowledge of the quenching mechanism is very important as it may provide hints on how to functionalize ligands and to tune and improve their luminescence performance.

The interaction of molecular solvent with solute molecules can be examined using different experimental techniques, whose applicability and/or accuracy is however limited in the presence of protic solvents like water. The combination of neutron and X-ray diffraction is nowadays the best approach to study the molecular structure of aqueous solutions and the interaction of water molecules and a solute.[17] The experimental data obtained using these techniques can be applied to constrain Monte Carlo based atomistic simulations, e.g. using the Empirical Potential Structure Refinement (EPSR) method.[18] EPSR is an iterative algorithm that minimises the energy of the system while building an atomistic model that is consistent with the experimental data. EPSR maximises the information obtainable from neutron and X-ray diffraction data, and the results can then be compared directly with more traditional theoretical methods, including electronic structure first-principles approaches. The combination of neutron scattering and EPSR simulations has been used for many years to study molecular liquids and aqueous solutions, in particular. More recently, this technique, in combination with ab initio simulations, was used for the first time to determine interactions between metal complexes and water molecules in solution in a homogeneous catalytic system.[19]

[a] Dr. F. Scalambra, Prof. Dr. A. Romerosa
Área de Química Inorgánica-CIESOL
Universidad de Almería
Carretera Sacramento s/n, Almería, Spain.
E-mail: romerosa@ual.es

[b] Dr. Nicole Holzmann
Scientific Computing Department
STFC Rutherford Appleton Laboratory
Harwell Oxford, Didcot, OX11 0QX, UK

[c] Dr. Leonardo Bernasconi
Center for Research Computing
University of Pittsburgh
312 Schenley Place, 4420 Bayard Street, Pittsburgh, PA 15260, USA

[b] Dr. Silvia Imberti
ISIS Neutron and Muon Source
STFC Rutherford Appleton Laboratory
Harwell Oxford, Didcot, OX11 0QX, UK

Supporting information for this article is given via a link at the end of the document.

In 2014 we presented the first study of an aqueous solution of the organometallic complex [RuCp(PTA)$_2$–μ-CN–1κ*C*:2k^2*N*-RuCp-(PTA)$_2$](CF$_3$SO$_3$) based on a combination of neutron and X-ray scattering, experimental UV-Vis and time-dependent density-functional theory (TDDFT) calculations. We showed that only after an EPSR-based structural refinement of solute configurations determined from neutron scattering data, were the calculated UV-vis spectra is in agreement with their experimental counterparts. The electronic absorption spectra of the complex in protic and aprotic solvents were found to be different, owing to differences in the nature of the interactions of water molecules with the lipophilic cyclopentadienyls.[14]

On the basis of these findings, we use here a similar combination of neutron data, EPSR and TDDFT calculations to study the absorption and the water environment in complexes *cis*-{Ru(bpy)$_2$(PTA)$_2$}$^{2+}$ (**1**) and *trans*-{Ru(bpy)$_2$(PTA)$_2$}$^{2+}$ (**2**) (Figure 1). We are particularly interested in understanding why these complexes have a promising but low fluorescence yield in aqueous solution and how this can be improved.

The solubility in water to achieve the required concentration for neutron and X-ray scattering experiments was sufficient for complex **1Cl$_2$** but not for the previously published **2(CF$_3$SO$_3$)$_2$**. Therefore, a more soluble salt of **2** was needed to be synthesised. The fluoride salt of *trans*-[Ru(bpy)$_2$(PTA)$_2$]$^{2+}$ (**2F$_2$**) was found to be the most adequate compound for neutron measurements, as displays good solubility in water and the counter ion is also a halogen. In this study we describe an investigation of aqueous solution of *cis*-[Ru(bpy)$_2$(PTA)$_2$]Cl$_2$ (**1Cl$_2$**) and *trans*-[Ru(bpy)$_2$(PTA)$_2$]F$_2$ (**2F$_2$**) based on neutron diffraction measurements and TDDFT calculations.

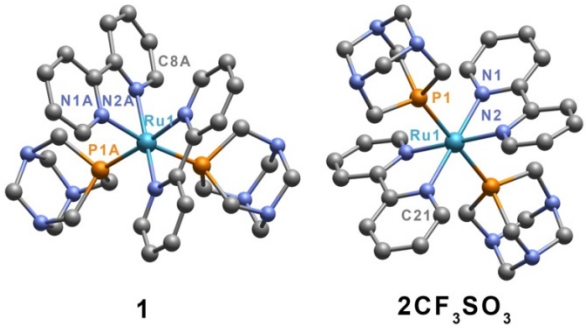

Figure 1. Representation of the crystal structure of **1** and **2(CF$_3$SO$_3$)$_2$**.[14]

Results and Discussion

Synthesis of 1Cl$_2$ and 2F$_2$.

The previously reported synthesis of **1Cl$_2$** and **2(CF$_3$SO$_3$)$_2$** was used to obtain these complexes in good yield and in quantities sufficient for their general characterisation. Larger yields were however required for the neutron and X-ray experiments. For this reason, and to guarantee a homogeneous composition of the samples a new synthesis procedure has been developed, which can yield up to 3-4 g of product in a single batch. As indicated in the Introduction, a salt of **2** more soluble in water than the triflate is required to achieve a concentration suitable for neutron scattering experiments and if possible with a similar counter ion to that for **1**. The fluoride salt of **2** displays a solubility in water ten times higher than the triflate salt (**2(CF$_3$SO$_3$)$_2$**: $S_{25°C}$ = 110 mg/cm^3; **2F$_2$** = $S_{25°C}$ = 1040 mg/cm^3).

Complex **2F$_2$** was synthesized upon treatment of a solution of **2(CF$_3$SO$_3$)$_2$** in water with NBu$_4$F. The purity of the compounds obtained with these scaled up procedures was confirmed by ^{1}H, ^{31}P{^{1}H} and ^{13}C{^{1}H} ^{15}F{^{1}H} NMR, IR spectroscopy. Complex **2F$_2$** showed identical spectra to those of **2(CF$_3$SO$_3$)**, apart from the CF$_3$SO$_3$ bands in the IR and the ^{15}F signals in NMR. Finally, the structure of **2F$_2$** was confirmed by single crystal X-ray diffraction. In addition to the spectroscopic check of the purity of the complexes, a powder X-ray diffraction experiment supported the homogeneity of the samples used in the neutron and X-ray experiments.

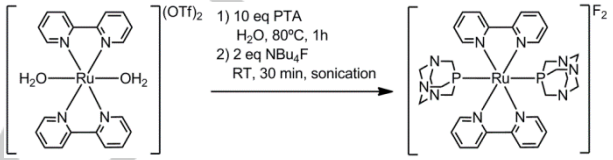

Scheme 1. Synthesis of **2F$_2$**.

Crystal structure of 2F$_2$.

Diffusion of acetone in an aqueous solution of **2F$_2$** at room temperature produced yellow crystals. All attempts to obtain single crystal were unsuccessful. Nevertheless, some obtained twinned crystals were recorded by using single crystal X-ray diffraction, being the data good enough for determining the crystal structure of the complex. Analysis of the data showed that the unit cell contains two cationic complexes *trans*-{Ru(bpy)$_2$(PTA)$_2$}$^{2+}$, four F$^-$ and 24 water molecules. The ruthenium atom displays a distorted octahedral coordination sphere constituted by two PTA ligands *trans* to each other, which are coordinated through their P atoms, and two bpy ligands also *trans* to each other (Figure 2). The most important

Table 2. Selected bond distances and angles of **2F$_2$**.

Ru1-P1	2.341(2) Å
Ru1-P2	2.332(2) Å
Ru1-N7	2.104(4) Å
Ru1-N8	1.092(4) Å
Ru1-N9	2.100(4) Å
Ru1-N10	2.102(4) Å
P1-Ru1-N7	91.9(1)°
P1-Ru1-N8	91.6(1)°
P1-Ru1-N9	89.3(1)°
P1-Ru1-P2	179.34(6)°

interatomic distances and angles are given in Table 1 and are

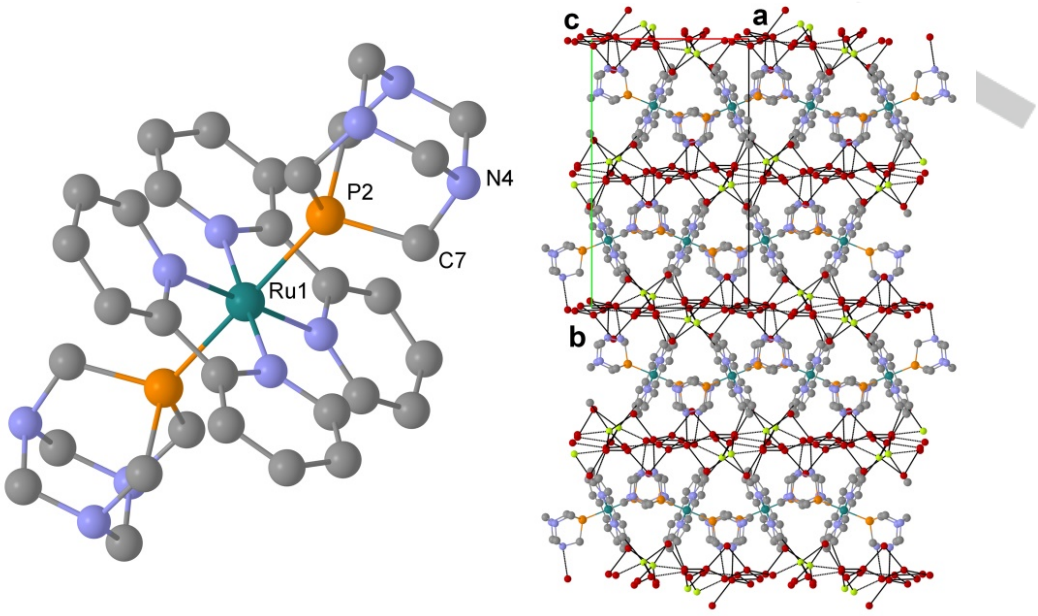

Figure 2. Asymmetric unit of **2F₂** (left) and crystal packing showing hydrogen bond network (right). Hydrogen atoms are not included for clarity.

similar to those published for complex **2(CF₃SO₃)**.[14] The Ru-P and Ru-N bond lengths are somewhat shorter in **2F₂** (Ru-P1 = 2.342(18) Å, 2.353(18) Å; Ru-N range: 2.105(5) Å - 2.110(5) Å), and agree with previously reported bisbipyridine-bisphosphine ruthenium complexes. [23] The Ru-P distances are similar to those observed in *trans*-[$RuCl_2(PTA)_4$] (2.317(2) Å – 2.353(2) Å), indicating lower steric impediment in **2**. The largest and smallest angles of the complex around Ru in **2F₂** (P1-Ru1-N10 = 87.9(1)º; P1-Ru1-N7 = 91.9(1)º) show that the coordination geometry in this complex is slightly more distorted than in **2CF₃SO₃** (P1-Ru1-N1 = 91.30(14)º; P1-Ru1-N2 = 88.90(14)º), while distortion of the bpy rings remain similar each other and with previously reported complexes.[24] The packing of **2F₂** is constituted by monolayers containing complex molecules alternated with monolayers of water perpendicularly to the cell *c* axis, which are connected by hydrogen bonds involving the nuclei N2-O12, N4-O7. Additionally, an extended hydrogen bond network connects the water molecules among them and to the fluoride anions (Figure 2).

In addition to the elemental analysis, the number of water molecules in the crystalline sample was confirmed through additional measurements. Thermogravimetric analysis under N_2 atmosphere confirmed that, upon warming 12 water molecules per complex are eliminated, which corresponds to the water molecules belonging to the crystal structure of **2F₂**. The process occurs in four steps from 41ºC to 206ºC (Figure S1). The observed starting temperature for the process agrees with what found for other water-hosting systems containing PTA.[22]

UV-vis spectra of 1Cl₂ and 2F₂

2.341(2) Å, Ru1-P2 = 2.332 (15) Å; Ru-N range: 2.092(4) Å-2.104(4) Å) than in **2CF₃SO₃** (Ru-P:

The electronic spectrum of **1Cl₂** in water has been characterized and discussed previously. [14] When DMSO replaces water, three main absorption bands arise at 261 nm, 298 nm and 417 nm (Figure 3), which show an irregular bathochromic shift with respect to their analogues in water. The band molar absorption coefficients of **1Cl₂** in DMSO show a general hypochromism with respect to the absorptions found in water ($\varepsilon_{(261,\ DMSO,\ 25ºC)}$ = 9854 $dm^3 \cdot mol^{-1} \cdot cm^{-1}$, $\varepsilon_{(203,\ H2O,\ 25ºC)}$ = 74965 $dm^3 \cdot mol^{-1} \cdot cm^{-1}$; $\varepsilon_{(298,\ DMSO,\ 25ºC)}$ = 13032 $dm^3 \cdot mol^{-1} \cdot cm^{-1}$, $\varepsilon_{(298,\ H2O,\ 25ºC)}$ = 24356 $dm^3 \cdot mol^{-1} \cdot cm^{-1}$; $\varepsilon_{(417,\ DMSO,\ 25ºC)}$ = 2105 $dm^3 \cdot mol^{-1} \cdot cm^{-1}$, $\varepsilon_{(417,\ H2O,\ 25ºC)}$ = 4517 $dm^3 \cdot mol^{-1} \cdot cm^{-1}$).

The UV-vis spectrum of **2F₂** in water (Figure 3) is identical to that found for **2CF₃SO₃**, both in number and shape of bands and their absorption coefficient. The spectra is constituted by three main bands at 213 nm, 288 nm and 425 nm and a shoulder at 245 nm (**2F₂**: $\varepsilon_{(213,\ H2O,\ 25ºC)}$ = 70032 $dm^3 \cdot mol^{-1} \cdot cm^{-1}$, $\varepsilon_{(288,\ H2O,\ 25ºC)}$ = 29019 $dm^3 \cdot mol^{-1} \cdot cm^{-1}$ and $\varepsilon_{(425,\ H2O,\ 25ºC)}$ = 5951.1 $dm^3 \cdot mol^{-1} \cdot cm^{-1}$; **2CF₃SO₃:** $\varepsilon_{(213,\ H2O,\ 25ºC)}$ = 70533 $dm^3 \cdot mol^{-1} \cdot cm^{-1}$, $\varepsilon_{(288,\ H2O,\ 25ºC)}$ = 29784 $dm^3 \cdot mol^{-1} \cdot cm^{-1}$ and $\varepsilon_{(425,\ H2O,\ 25ºC)}$ = 6450 $dm^3 \cdot mol^{-1} \cdot cm^{-1}$).[14] Therefore the counterion produces minimal or no effects on the electronic spectra of complex cation **2** in solution. In DMSO the electronic spectrum of **2F₂** (Figure 3), similarly to that observed for **1Cl₂**, shows a general bathochromic effect as the main absorptions are moved to 260 nm, 299 nm and 457 nm, while a hypocromic effect is observed in the absorption coefficient, which is more pronounced for the bands at higher energy ($\varepsilon_{(260,\ DMSO,\ 25ºC)}$ = 21441 $dm^3 \cdot mol^{-1} \cdot cm^{-1}$, $\varepsilon_{(299,\ DMSO,\ 25ºC)}$ = 26880 $dm^3 \cdot mol^{-1} \cdot cm^{-1}$ and $\varepsilon_{(417,\ DMSO,\ 25ºC)}$ = 5834 $dm^3 \cdot mol^{-1} \cdot cm^{-1}$).

Interestingly, except for the region between 350 and 500 nm, the UV-vis spectra of **1Cl₂** and **2F₂** in DMSO are almost identical

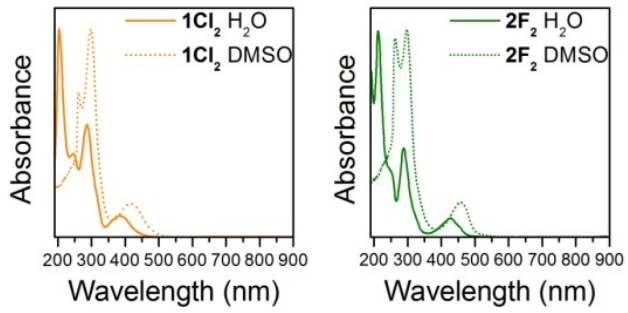

Figure 3. Absorption spectra of **1Cl₂** (left) and **2F₂** (right) in water and DMSO.

while in H_2O (Figure 3) they are significantly different, which indicates the existence of sizable interactions of water molecules with both complexes

Theoretical calculations.

Complexes **1** and **2** were optimized in the gas phase and in aqueous solution. Selected bond distances and angles are given in Tables S2 and S3. The overall agreement with experimental structures [14] is satisfactory although a small overestimation of the bond distances is observed. Absorption peaks in calculated absorption spectra (Figure 4 and Table S4) of the gas phase isomers are predominantly located in the ultra violet region below 300 nm. Both spectra show a well-defined peak around 267 nm, while **1** spectrum also exhibits a second intense peak at 218 nm, which is redshifted to 235 nm for **2**. A close inspection of the calculated transitions in terms of orbital excitations and the corresponding orbital shapes explains the difference in the peak energies.

Phosphine ligands like PTA are commonly known for their strong σ donation ability.[23] Thus, a strong interaction of the two σ orbitals on the PTA ligands with the d orbitals of the ruthenium coordination centre is not surprising. Indeed, as it can be seen in the LUMO+6 of both isomers (Figure 5), the d_{z2} orbital of ruthenium is oriented along the axis of the PTA phosphines in **2**, whereas it is pointing toward two of the bipyridine nitrogens in **1**.

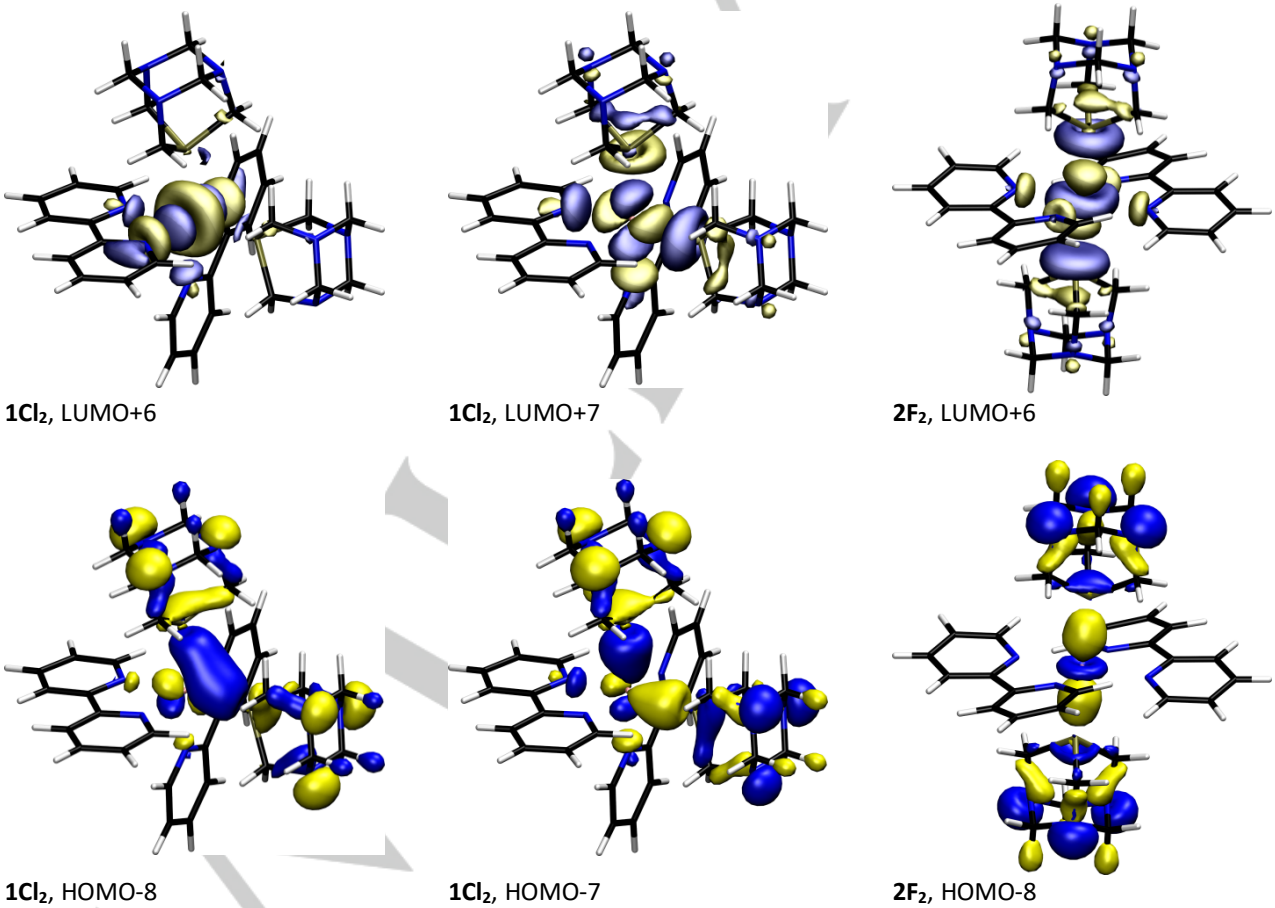

Figure 5. Selected orbitals of **1Cl₂** and **2F₂**. from calculations at B3LYP/def2-TZVPP.

The strong interaction of the d_{z2} with the phosphine σ(+,+) orbital (resulting orbital from the in-phase combination of the σ orbitals of the two individual phosphines) leads to hybridisation resulting in two molecular orbitals (HOMO-8 and LUMO+6, the latter being the anti-bonding counterpart of the former) with mixed contribution from the ruthenium d_{z2} and the PTA σ(+,+) orbital for **2**. In isomer **1**, HOMO-8 is dominated by the phosphine σ(+,+) orbital complementary to the LUMO+6 of predominantly d_{z2} character, but no orbital mixing is observed. Instead, the phosphine σ(+,-) orbital (resulting from the out-of-phase combination of the σ orbitals of the two individual phosphines) overlaps with the d_{x2-y2} ruthenium orbital along the Ru-P bonds. The resulting hybridised molecular orbitals for **1** are HOMO-7 (bonding) and LUMO+7 (anti-bonding, Figure 5). None of the aforementioned orbitals are part of the immediate frontier orbital region. However, the transition compositions of the calculated absorption spectra (Table S4 and S5) show that a direct HOMO to LUMO transition is not involved and that, overall, the four highest occupied and four lowest unoccupied orbitals only play a minor role.

The absorption peak at 218 nm in the electronic spectrum of **1** primarily stems from a transition between HOMO-8 and LUMO+7. The latter shows electron density regions localised both at the Ru centre and along the bonds between Ru and the ligands. The second transition (HOMO-12 to LUMO) corresponds to two orbitals with electron density at the ligands. Thus, this excitation can be described as LMCT/LLCT (ligand-to-metal and ligand-to-ligand charge transfer) excitation. By contrast, the absorption peak at 235 nm in the spectrum of **2** originates from a transition from the ligand based σ(+,-) HOMO-4 to the d_{z2} symmetric LUMO+6 (and another ligand-to-ligand transition, HOMO-1 to LUMO+11). Although this can also be described as a LMCT/LLCT excitation, the symmetry of the participating orbitals is fundamentally different.

The overlapping peaks at 267 nm in the **1** and **2** absorption spectra correspond to transitions with partial LLCT character. An additional contribution from a MLCT excitation (d_{xy} HOMO-6 on Ru to the bipyridine ligand orbital LUMO+5 in **1**, and d_{xz} HOMO-7 on Ru to the bipyridine LUMO+4 in **2**) is also observed. In both these Ru centred d orbitals the lobes are slightly deformed and pointing towards the phosphine π orbitals. In addition to being a strong σ donor, phosphine ligands show considerable π acceptor ability, which is related by the presence of low lying unoccupied π orbitals on the P atom.

These findings suggest that the electronic structure, and therefore the absorption spectra, of **1** and **2** are significantly affected by the strong σ donation and π accepting ability of the phosphine ligands, which should have a strong influence in the fluorescence of the complexes.

In terms of explicit water coordination around the complex, it is worth noting that the six lowest lying unoccupied orbitals (LUMO to LUMO+5) in both **1** and **2** all exhibit electron density at the bipyridyl ligands only, while in the four highest occupied orbitals (HOMO-3 to HOMO) the electrons are mainly located at the PTAs, but shared with smaller localisations at the ruthenium atom.

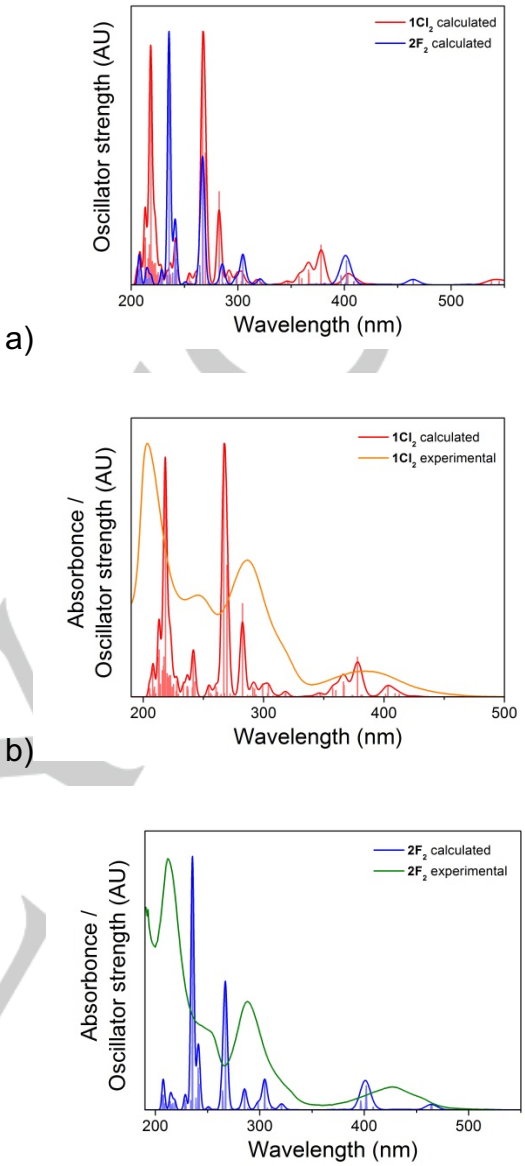

Figure 4. a) Detailed view of the ultra-violet region below 300 nm. b-c) comparison between the calculated and experimental spectra in water of **1Cl2** and **2F2**.

Water has two electron lone pairs located at oxygen that are represented by the two highest lying molecular orbitals HOMO ($1b_1$, out of plane p orbital shape at O) and HOMO-1 ($3a_1$, in plane p orbital shape at O) that both are prone to interact with the energetically accessible low lying unoccupied orbitals. The less well pronounced localisation at PTA for the highest lying occupied orbitals show, as expected, distinctive lobes at the PTA nitrogen atoms, which exhibit a free electron pair in this positions. These can potentially interact with the low lying

unoccupied water orbitals, forming hydrogen bonds. However, the quite small negative calculated Mulliken charge of -0.15 at nitrogen (compared to -0.75 at nitrogen in gas phase ammonia[24]) does not indicate a strong driving force for the formation of hydrogen bonds. Electronic excitation, that shifts electron density into the unoccupied bipyridyl located orbitals is thus likely to affect the water orientation and coordination around these complexes.

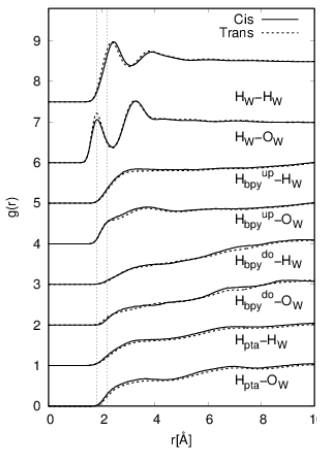

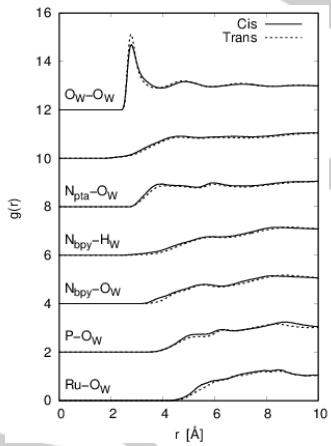

Figure 6: A selection of site-site pair distribution functions (PDF) or g(r)s for water oxygen Ow around relevant sites on compounds 1Cl2 (cis, full line) and 2(CF3SO3)2 (trans, broken line). The PTA ligand atoms are labelled "pta", while the bipyridine is labelled "bpy". Cup, Cdo, Hup, Hdo are sites on the bipyridine ligands (labelled according to their charges, as detailed in the supporting information). Labelled CC_{bpy} are the carbon atoms connecting the two rings, C_{bpy} all the other atoms on the bipyridine rings. Water-water correlations are also presented.

Neutron/X-ray Diffraction and EPSR Simulations.

Neutron diffraction enhanced by hydrogen/deuterium isotopic substitution (NDIS)[17] and high energy (Ag source) X-ray diffraction[35] has been used to study a 0.5 M solution of **$1Cl_2$** and **$2F_2$** in water. EPSR simulations have been run from a starting potential, reported in detail in Table S6 in the Supporting Information. Four experimental patterns (X-rays, neutrons on H_2O, D_2O and the equimolar mixture) have been used to simultaneously refine the initial potential until a satisfactory comparison with the experimental data has been achieved. The comparison between experimental and simulated structure factors can be inspected in Figure S7 in the Supporting Information. From the simulation boxes for *cis* and the one for *trans*, the site-site pair distribution functions (PDF), or radial distribution functions g(r)s, have been extracted, containing information about the most likely, nearest-neighbour positions for all the atomic pairs in the simulation box. A selection of the most relevant g(r)s for the following discussion is shown in Figure 6.

As a general comment, as it can be seen from the superposition of the g(r)s for the two compounds, the solute-water correlations are very similar to each other. The presence of a large number of water molecules around the solute, although distributed, is compatible with the good solubility in water of these compounds. Similarly, for the water-water correlations, there are no significant differences between the two compounds, and an excluded volume effect is clearly present (water-water g(r)s slightly raised towards the r=0). This reflects the fact that the partial charges assigned to each ligand do not vary greatly between the two compounds. As a matter of fact, the partial charges used in the EPSR simulation – partly modified from an original set of Mulliken charges (see Table S6 and Figure S9 in the supporting information)– do show only a small difference between the *cis* and *trans* complexes, specifically in the way the carbon charges are distributed around the rings. This is consistent with the fact that the orbitals structure between complexes **1** and **2**, although sufficient to produce the modification of the electronic distribution in the molecule and therefore induce optical effects, is not significant enough to provide a strong difference in the hydration of these compounds.

The bipyridine groups have slightly more pronounced polarity than the PTA ligands, and, as a consequence, a slightly more pronounced solute-water correlations (see H_{up}-Ow and H_{up}-Hw g(r)s versus the corresponding H_{PTA}-Ow g(r) in Figure 4). It is interesting to note that the water oxygen and hydrogen around the "up" hydrogens of the bipyridine group (the ones with slightly stronger partial charge) are oriented with the water dipole pointing outwardly, as in the water-water hydrogen bonding correlation (also reported in the same figure). The slightly enhanced presence of water around the bipyridine groups, is compatible with the LUMO orbitals occupancy (see Figure S6, e.g. LUMO to LUMO+5) in the ground state, that are mainly concentrated around these ligands rather than around the PTA ligands. We do in fact expect the water oxygen orbital (lone pair) to interact predominantly (and easily, due to low steric

hindrance of the water molecule) with the LUMO orbitals on the bipyridine.

Conclusions

Despite similar compositions, the complexes **1Cl₂** and **2F₂** are coordination isomers, which imparts them significantly different optical properties in water, as showed in their electronic spectra. The *cis*-complex **1**, in which the PTA ligands are close together, and the *trans*-complex **2** have different orbital symmetries in the PTA's σ and π electron donation and back-donation, resulting in molecular orbitals that are energetically similar but differ significantly in electron density distribution around the Ru ion. According to our neutron scattering data and DFT calculations, these differences can be attributed to steric effects, as the *cis*-complex has more space available for the interaction with water molecules in the empty region between the two adjacent bipyridine ligands. These small differences are not sufficient to modify measured g(r)s appreciably, since several sites are averaged together. The full 3D (EPSR + DFT) information analysis, despite its computational cost, is therefore essential to highlight sites for solute-solvent interaction.

These differences in the Ru coordination environment are reflected in the energies and distributions of the metal centre and ligand orbitals, which modify the overall charge on the individual atoms in the complexes. For instance, the calculated Mulliken charges indicate a larger positive charge in the outer section of the bipyridine rings. In turn, these effects result in a different response to UV-vis radiation. Both experimental and calculated optical spectra indicate a substantial difference between the *cis* and *trans* isomers, with the lowest absorption band decreasing by ca. 50 nm in the *trans* isomer relative to the *cis* one. According to our orbital analysis, the low energy region of the UV-vis spectrum (350-450 nm) is dominated by charge-transfer electronic transitions, whose energy is sensitive to the coordination environment of the orbitals involved in the transition. In the case of the *cis* isomer, the presence of a larger number of water molecules in the immediate vicinity of the excited-electron orbital, orienting the negative end of their dipole moment vector toward it, destabilises *via* charge-dipole interaction (and/or Pauli repulsion with the excited electron) the charge transfer process, resulting in the observed hypsochromic shift in the absorption spectra (Figure 3).

In summary, we have presented a study of the hydration of **1** and **2** based on neutron scattering data, UV-vis measurements and EPSR/TD-DFT calculations. Our results indicate that differences in the solvation environments of **1** and **2**, which are not captured by (coordination site averaged) PDFs alone, can be characterised using a spatial 3D analysis of the solvent distribution. The different solvation structures of **1** and **2** that are largely dominated by steric effects (solvent accessibility), are reflected in the optical response of the two isomers, particularly in the low energy region of their UV-vis spectra. On the basis of DFT and TD-DFT calculations, we attribute these spectral changes to the response of specific charge-transfer excitations to the presence of water molecules in the vicinity of the complex, which occupy free spatial domains made accessible by a *trans*-*cis* conformational change. Experiments and additional calculations are in progress to determine if the fluorescence properties of theses complexes are also determined by the same effects.

Experimental Section

General Procedures

All chemicals were reagent grade and, unless otherwise stated, were used as received from commercial suppliers. Likewise, all reactions were carried out in a pure nitrogen atmosphere by using standard Schlenk-tube techniques. The water used was of milliQ grade. The ligand PTA and complexes *cis*-$[Ru(bpy)_2Cl_2]\cdot 2H_2O$ and *trans*-$[Ru(bpy)_2(H_2O)_2](CF_3SO_3)_2$ were prepared as described in the literature.[14,25,26]

Synthesis of *cis*-$[Ru(bpy)_2(PTA)_2]Cl_2$ (1Cl₂)

In the dark and under nitrogen, complex *cis*-$[Ru(bpy)_2Cl_2]\cdot 2H_2O$ (2.6 g, 5 mmol) was suspended in 50 mL of deoxygenated water and refluxed during 15 min. ligand PTA (3.93 g, 25 mmol) was added in small portions (<0.1 g) and the resulting solution was let to reflux during 2.5 h. The deep orange solution obtained was filtered through celite and the solved removed under reduced pressure to give an orange powder, which was stirred in acetone/Et_2O 1:1.5 (30 mL) during 30 min, filtered, washed with acetone (3x20 mL) and dried under vacuum. Yield = 3.63 g (91%).

Synthesis of *trans*-$[Ru(bpy)_2(PTA)_2]F_2$ (2F₂)

In the dark and under nitrogen, complex *trans*-$[Ru(bpy)_2(H_2O)_2](CF_3SO_3)_2$ (4 g, 5.6 mmol) and PTA (8.83 mg, 56 mmol) were suspended in 120 mL of deoxygenated water and then warmed at 80 ºC. After 1hthe solution was cooled, NBu_4F (2.93 g, 11.2 mmol) was added and the mixture sonicated during 30 min and then filtered. The filtrate was concentrated to 10 mL, kept at 4ºC overnight and filtered again to remove any residual $NBu_4CF_3SO_3$. The resulting solution has been evaporated to dryness under reduced pressure and the obtained solid was washed by stirring in acetone (3 x 30 mL) during 30 min. The obtained orange powder was filtered and dried under vacuum. Yield: 3.82 g mg (89%). Elemental analysis for $C_{34}H_{40}F_6N_{10}O_6P_2S_2Ru$ (1026,10): Found C, 39.69; H, 4.19; N, 13.35; S, 5.95; calcd. C, 39.81; H, 3.93; N, 13.65; S, 6.25. ^{1}H NMR (300.13 MHz, D_2O, 25 ºC): δ 3.14 (s, 24H, PCH_2N_{PTA}); 3.96 (d, $^2J_{HH}$=13.23 Hz, 12H, NCH_2N_{PTA}); 4.17 (d, $^2J_{HH}$=13.21 Hz, 6H, NCH_2N_{PTA}); 7.81 (m, 4H, 5-bpy); 8.28 (m, 4H, 4-bpy); 8.55 (m, 4H, 3-bpy); 9.32 (m, 6H, 6-bpy). $^{13}C\{^1H\}$ NMR (75.47 MHz, D_2O, 25ºC): δ 45.78 (t, $^2J_{PC}$ = 11 Hz, $^4J_{PC}$ = 3 Hz, NCH_2P_{PTA}); 70.24 (s, NCH_2N_{PTA}); 124.77 (s, 3-bpy); 127.32 (s, 5-bpy); 139.61 (s, 4-bpy); 153.48 (s, 6-bpy); 157.34 (s, 2-bpy). $^{31}P\{^1H\}$ NMR (121.49 MHz, D_2O, 25ºC): δ -50.53 (PTA). $^{19}F\{^1H\}$ NMR (282.40 MHz, D_2O, 25ºC): δ -121.9 (broad, F^-); -129.9 (s, F^-). UV-vis (H_2O, 25ºC): nm [ε ($dm^3\ mol^{-1}\ cm^{-1}$)]: 212 [70032], 288 [29019], 427 [5951]; UV-vis (DMSO, 25ºC): nm [ε ($dm^3\ mol^{-1}\ cm^{-1}$)]: 260 [21441], 299 [26880], 457 [5834].

Theoretical Methods

Theoretical calculations were carried out using the NWChem6.6 program package[27]. Ground state optimised structures were obtained using density-functional theory (DFT) at the B3LYP/def2-TZVPP level of

theory.[28–30] For gas phase vertical excitations the TDDFT method was applied with the smaller def2-SVP basis set.[31] Absorption spectra were calculated considering the 130 lowest singlet excited states. The 'COnductor-like Screening MOdel' (COSMO), as implemented in NWChem6.6, was used to describe water, with a dielectric constant ε_{H2O} = 78.0.[32] In all calculation the def2-ecp effective core potential was used for Ru.[33]

Neutron diffraction experiments

A 0.5 M solution of **1Cl$_2$** or **2(CF$_3$SO$_3$)$_2$** in H_2O, D_2O or 1:1 molar H_2O/D_2O ("HDO") has been prepared to be used for the neutron and X-ray diffraction experiments. For neutron experiments each freshly prepared solution has been syringed to flat TiZr alloy cans at 25ºC (sample thickness 1 mm). For X-rays measurements, 1 mm fused quartz capillary tubes were charged with the freshly prepared solution of **1Cl$_2$** or **2(CF$_3$SO$_3$)$_2$**. The neutron experiments have been performed on SANDALS diffractometer at the ISIS spallation neutron source, located at the Rutherford Appleton Laboratory (United Kingdom). The neutron data have been corrected for detectors efficiency, attenuation, multiple scattering, and inelastic scattering using well established methods.[34] White beam X-ray diffraction data have been collected on a Panaytical Ag-source diffractometer also available at ISIS. High-energy X-ray data were corrected for detector efficiency, polarization, Compton scattering and fluorescence.[35] Computational models of the system have been obtained through Empirical Potential Structure Refinement (EPSR)[36] and implemented with EPSRgui.[37] The simulation boxes contain 20 solute and 1100 solvent molecules, at the density of 0.1 atoms/Å^3. The coulomb term of the interaction potential and molecular structure of **1Cl$_2$** and **2(CF$_3$SO$_3$)$_2$** have been determined from the ab initio atomic structure in the gas phase and from the corresponding Mulliken population charges, both computed at the B3LYP level of DFT. The Lennard-Jones term of the interaction potential for the solutes was freely adapted from Jorgensen.[38] For the water molecules a classic SPC/E[39] model has been adopted.

Acknowledgments

We acknowledge the Project CTQ2015-67384-R (MINECO) that have been funded by the FEDER program, the PAI group FQM-317 and the COST Action CM1302 (WG1, WG2). Beamtime with the RB number 1510513 on the ISIS neutron and muon source (STFC) is also acknowledged (data available online at DOI: 10.5286/ISIS.E.58448680). NH and LB acknowledge support from the UK HPC Materials Chemistry Consortium (grant EP/L000202) and from the EPSRC Service Level Agreement with STFC Scientific Computing Department.

Keywords: Ruthenium, triazaphosphaadamantane, bibyridine, water-soluble complexes, neutron scattering, TDDFT.

[1] T. Nandhini, K. R. Anju, V. M. Manikandamathavan, V. G. Vaidyanathan, B. U. Nair, *Dalt. Trans.* **2015**, *44*, 9044–9051.
[2] B. S. Howerton, D. K. Heidary, E. C. Glazer, *J. Am. Chem. Soc.* **2012**, *134*, 8324–8327.
[3] E. Wachter, D. K. Heidary, B. S. Howerton, S. Parkin, E. C. Glazer, *Chem. Commun.* **2012**, *48*, 9649–9651.
[4] Y.-Q. Zou, J.-R. Chen, X.-P. Liu, L.-Q. Lu, R. L. Davis, K. A. Jørgensen, W.-J. Xiao, *Angew. Chemie Int. Ed.* **2012**, *51*, 784–788.
[5] P. Wang, S. M. Zakeeruddin, J. E. Moser, M. K. Nazeeruddin, T. Sekiguchi, M. Grätzel, *Nat. Mater.* **2003**, *2*, 402–407.
[6] A. Wołoszyn, C. Pettinari, R. Pettinari, G. V. Badillo Patzmay, A. Kwiecień, G. Lupidi, M. Nabissi, G. Santoni, P. Smoleński, *Dalt. Trans.* **2017**, *46*, 10073–10081.
[7] J. Huang, J. Chen, H. Gao, L. Chen, *Inorg. Chem.* **2014**, *53*, 9570–9580.
[8] B. G. Hashiguchi, K. J. H. Young, M. Yousufuddin, W. A. Goddard, R. A. Periana, *J. Am. Chem. Soc.* **2010**, *132*, 12542–12545.
[9] I. Nieto, M. S. Livings, J. B. Sacci, L. E. Reuther, M. Zeller, E. T. Papish, *Organometallics* **2011**, *30*, 6339–6342.
[10] R. Kawahara, K. Fujita, R. Yamaguchi, *J. Am. Chem. Soc.* **2012**, *134*, 3643–3646.
[11] Y. Himeda, N. Onozawa-Komatsuzaki, S. Miyazawa, H. Sugihara, T. Hirose, K. Kasuga, *Chem. - A Eur. J.* **2008**, *14*, 11076–11081.
[12] Y. Himeda, *Eur. J. Inorg. Chem.* **2007**, *2007*, 3927–3941.
[13] M. Bräutigam, M. Wächtler, S. Rau, J. Popp, B. Dietzek, *J. Phys. Chem. C* **2012**, *116*, 1274–1281.
[14] F. Scalambra, M. Serrano-Ruiz, S. Nahim-Granados, A. Romerosa, *Eur. J. Inorg. Chem.* **2016**, *2016*, 1528–1540.
[15] G. E. Dobretsov, T. I. Syrejschikova, N. V. Smolina, *Biophysics (Oxf).* **2014**, *59*, 183–188.
[16] N. Agmon, *J. Phys. Chem. A* **2005**, *109*, 13–35.
[17] J. L. Finney, A. K. Soper, *Chem. Soc. Rev.* **1994**, *23*, 1–10.
[18] A. K. Soper, *Mol. Simul.* **2012**, *38*, 1171– 1185.
[19] F. Scalambra, N. Holzmann, L. Bernasconi, S. Imberti, A. Romerosa, *ACS Catal.* **2018**, *8*, 3812–3819.
[20] A. C. Hazell, A. Mukhopadhyay, IUCr, *Acta Crystallogr. Sect. B Struct. Crystallogr. Cryst. Chem.* **1980**, *36*, 1647–1649.
[21] A. W. Cordes, B. Durham, P. N. Swepston, W. T. Pennington, S. M. Condren, R. Jensen, J. L. Walsh, *J. Coord. Chem.* **1982**, *11*, 251–260.
[22] F. Scalambra, M. Serrano-Ruiz, A. Romerosa, *Dalt. Trans.* **2018**, *47*, 3588–3595.
[23] F. A. Cotton, G. Wilkinson, M. Bochmann, *Advanced Inorganic Chemstry*, **1999**.
[24] R. Balawender, B. Safi, P. Geerlings, *J. Phys. Chem. A* **2001**, *105*, 6703–6710.
[25] D. J. Daigle, T. J. Decuir, J. B. Robertson, D. J. Darensbourg, *Inorg. Synth.* **1998**, *32*, 40–45.
[26] D. J. Daigle, A. B. Pepperman, S. L. Vail, *J. Heterocycl. Chem.* **1974**, *11*, 407–408.
[27] M. Valiev, E. J. Bylaska, N. Govind, K. Kowalski, T. P. Straatsma, H. J. J. Van Dam, D. Wang, J. Nieplocha, E. Apra, T. L. Windus, W. A. De Jong, *Comput. Phys. Commun.* **2010**, *181*, 1477–1489.
[28] A. D. Becke, *J. Chem. Phys.* **1993**, *98*, 1372–1377.
[29] C. Lee, W. Yang, R. G. Parr, *Phys. Rev. B* **1988**, *37*, 785–789.
[30] F. Weigend, R. Ahlrichs, *Phys. Chem. Chem. Phys.* **2005**, *7*, 3297.
[31] A. Dreuw, M. Head-Gordon, *Chem. Rev.* **2005**, *105*, 4009–4037.
[32] A. Klamt, G. Schüürmann, *J. Chem. Soc., Perkin Trans. 2* **1993**, *0*, 799–805.
[33] D. Andrae, U. Häussermann, M. Dolg, H. Stoll, H. Preuss, *Theor. Chim. Acta* **1990**, *77*, 123–141.
[34] A. Soper, *RAL Tech. Rep.* **2011**, RAL-TR-2011-013.
[35] A. K. Soper, E. R. Barney, IUCr, *J. Appl. Crystallogr.* **2011**, *44*, 714–726.
[36] A. K. Soper, *RAL Tech. Rep.* **2011**, RAL-TR-2011-012.
[37] S. Callear, *RAL Tech. Rep.* **2017**, RAL-TR-2017-002.
[38] W. L. Jorgensen, D. S. Maxwell, J. Tirado-Rives, *J. Am. Chem. Soc.* **1996**, *118*, 11225–11236.
[39] H. J. C. Berendsen, J. R. Grigera, T. P. Straatsma, *J. Phys. Chem.* **1987**, *91*, 6269–6271.

FULL PAPER

An analysis of the solvent distribution around the complexes, based on neutron diffraction data and *ab initio* calculations was used to study the solvent distribution around the two complexes, and to link the solvent environment to specific features in the optical response of their solutions.

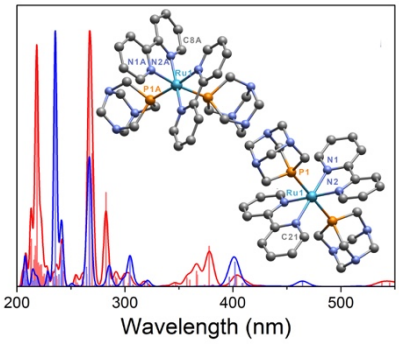

Neutron Scattering

*Franco Scalambra, Nicole Holzmann, Leonardo Bernasconi, Silvia Imberti, Antonio Romerosa**

Page No. – Page No.

The interaction of water with *cis* and *trans* {Ru(bpy)$_2$(PTA)$_2$}$^{2+}$ (PTA = 1,3,5-triaza-7-phosphaadamantane) studied by neutron scattering and *ab initio* calculations

*one or two words that highlight the emphasis of the paper or the field of the study

Water-Complex Interactions